Journal of Inorganic Biochemistry 112 (2012) 85–92

Contents lists available at SciVerse ScienceDirect

Journal of Inorganic Biochemistry

journal homepage: www.elsevier.com/locate/jinorgbio

EXAFS and NRVS Reveal a Conformational Distortion of the FeMo-cofactor in the MoFe Nitrogenase Propargyl Alcohol Complex

Simon J. George [a,b,*], Brett M. Barney [d,1], Devrani Mitra [c], Robert Y. Igarashi [d,2], Yisong Guo [c], Dennis R. Dean [e], Stephen P. Cramer [a,b], Lance C. Seefeldt [d]

[a] Department of Chemistry, University of California, Davis, CA 95616, USA
[b] Advanced Biological and Environmental X-ray Facility, Lawrence Berkeley National Laboratory, Berkeley, CA 94720, USA
[c] Department of Applied Science, University of California, Davis, CA 95616, USA
[d] Department of Chemistry and Biochemistry, Utah State University Logan, UT 84322, USA
[e] Department of Biochemistry, Virginia Polytechnic Institute and State University, Blacksburg, VA 24061, USA

ARTICLE INFO

Article history:
Received 23 July 2011
Received in revised form 3 January 2012
Accepted 7 February 2012
Available online 15 February 2012

Keywords:
Nitrogenase
Nitrogen Fixation
Metalloprotein
X-ray Absorption Spectroscopy (XAS)
Extended Absorption Fine Structure (EXAFS)
Nuclear Resonant Vibrational Spectroscopy (NRVS)

ABSTRACT

We have used EXAFS and NRVS spectroscopies to examine the structural changes in the FeMo-cofactor active site of the α-70^{Ala} variant of *Azotobacter vinelandii* nitrogenase on binding and reduction of propargyl alcohol (PA). The Mo K-edge near-edge and EXAFS spectra are very similar in the presence and absence of PA, suggesting PA does not bind at Mo. By contrast, Fe EXAFS spectra show a clear and reproducible change in the long Fe-Fe interaction at ~3.7 Å on PA binding with the apparent appearance of a new Fe-Fe interaction at 3.99 Å. An analogous change in the long Mo-Fe 5.1 Å interaction is not seen. The NRVS spectra exclude the possibility of large-scale structural change of the FeMo-cofactor involving breaking the μ^2 Fe-S-Fe bonds of the Fe_6S_9X core. The simplest chemically consistent structural change is that the bound form of PA is coordinated at Fe atoms (Fe6 or Fe7) adjacent to the Mo terminus, with a concomitant movement of the Fe away from the central atom X and along the Fe-X bond by about 0.35 Å. This study comprises the first experimental evidence of the conformational changes of the FeMo-cofactor active site on binding a substrate or product.

1. Introduction

The mechanism of dinitrogen reduction by MoFe nitrogenase remains a key unsolved problem in biological inorganic chemistry [1,2]. Nitrogenases are bacterial enzyme systems whose physiological function is to catalyze the reduction of dinitrogen to ammonia with a concomitant reduction of $2H^+$ to H_2 and hydrolysis of MgATP [1,2]. Interestingly, they can also similarly reduce a large number of triply and doubly bonded molecules so that, for example, acetylene is reduced to ethylene, CN^- to NH_3 and CH_4, while azide is reduced to NH_3 and N_2. The MoFe nitrogenases comprise two separate proteins, the MoFe protein, which is responsible for substrate binding and reduction, and the Fe protein, which is an electron donor for the MoFe protein and the site of ATP hydrolysis. The MoFe-protein contains two types of metalloclusters: the active site FeMo-cofactor, and the [8Fe-7S] P-cluster, which functions to facilitate electron delivery from the Fe-protein to the FeMo-cofactor. The Fe-protein contains a single [4Fe-4S] cluster. During a catalytic cycle this protein associates and dissociates from the MoFe protein several times, each time delivering electrons from this cluster to the MoFe-protein in a reaction that is dependent on the hydrolysis of MgATP.

X-ray crystallography has revealed the FeMo-cofactor to be a unique [Fe_7S_9MoX-homocitrate] cluster [3,4], Scheme 1. However, inspection of this structure does not provide either an obvious location for substrate binding or any obvious insight to the mechanism of substrate reduction. The structure can be rationalized into two distinct regions where binding might occur. The first is the terminal Mo site, which is coordinated to 3 S, a histidine residue and to *R*-homocitrate, a bidentate carboxylate ligand that is essential for N_2 reduction activity. The other is the central trigonal prism Fe_6S_9X core, where X denotes a C, O or N interstitial atom. Clearly, substrate binding and reduction could occur at Mo or any of these Fe atoms. Unfortunately, further crystallographic studies aimed at resolving this question are limited by the inherent difficulty of preparing the enzyme in pure stable substrate bound states. Although there has been considerable success in our laboratories in preparing high yields of nitrogenase with substrates or intermediates

* Corresponding author at: Department of Chemistry, University of California, Davis, One Shields Avenue, Davis, CA 95616, USA. Tel.: +1 530 752 8900; fax +1 530 752 8995.
E-mail address: sjgeorge@ucdavis.edu (S.J. George).
[1] Present address: Department of Bioproducts and Biosystems Engineering, University of Minnesota, St. Paul, MN 55108, USA.
[2] Present address: Department of Chemistry, University of Central Florida, Orlando, FL 32816, USA.

0162-0134/$ – see front matter © 2012 Elsevier Inc. All rights reserved.
doi:10.1016/j.jinorgbio.2012.02.004

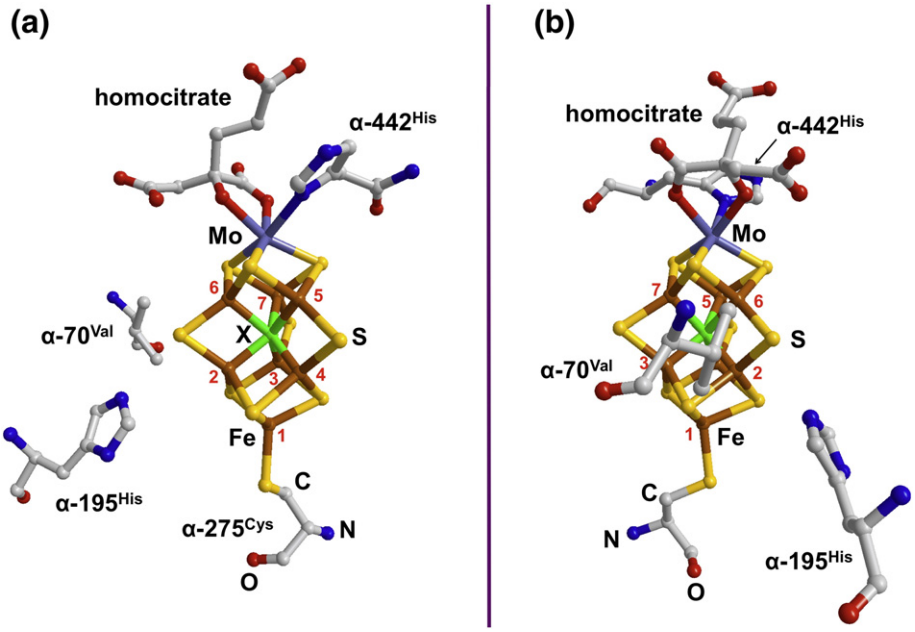

Scheme 1. The structure of the FeMo-cofactor drawn from PDB file 1M1N [3]. Mo – purple; Fe – brown; S – yellow, O – red; N – blue; C – grey; X – green. The Fe atoms are numbered in red.

bound to the FeMo-cofactor [5–8], these states are invariably transient and hence difficult if not impossible to crystallize. This problem is inherent to the enzyme; in order to bind substrates the enzyme needs to be in a reduced state, however, these reduced states tend to auto-oxidize to the resting state through H_2 evolution with concomitant substrate dissociation [1,2].

There are a number of mechanistic proposals, supported by density functional theory (DFT) calculations [9–12], and these in turn provide questions that can be experimentally addressed by spectroscopy. The first most obvious question is: do substrates initially bind at the Mo centre or at one or more of the Fe sites of the Fe_6S_9X core? Mechanisms focused on substrate binding to either Mo or Fe sites have both been proposed, as have approaches that involve migration of substrate-derived moieties between metal atoms during reduction [5–8]. Another question is whether substrate binding and reduction involves any conformational or structural change of the FeMo-cofactor. The Mo-based proposals often require dissociation of the homocitrate carboxylate concomitant with substrate binding [8,13]. The Fe-based proposals tend to exploit the unique chemical features of the Fe_6S_9X core of the cofactor, and conformational distortions and even core-opening through breaking Fe-S bonds are common features of the substrate bound reduced intermediates predicted by density functional theory (DFT) calculations [9–12].

X-ray absorption spectroscopy (XAS) combined with ^{57}Fe nuclear resonance vibrational spectroscopy (NRVS) offers a route to resolve these questions. Analyses of the extended x-ray fine structure (EXAFS) region of XAS spectra yield structural information, specifically numbers, distances and approximate element type of atoms adjacent to a specific absorbing element [14,15], while the near-edge region can give information about the ligand field. For MoFe nitrogenase, EXAFS not only has the potential to directly detect the coordination of bound ligands, but also to probe changes in FeMo-cofactor conformation from a study of the characteristic long-range ~5.1 Å Mo-Fe (Scheme 2b) and ~3.7 Å Fe-Fe interactions (Scheme 2c) across the cofactor Fe_6S_9X core. ^{57}Fe NRVS, a technique that exploits the Mössbauer effect, provides ^{57}Fe-specific vibrational spectra that extend from 10 cm^{-1} to approximately 500 cm^{-1}, and which are direct measurements of the motion of the resonant ^{57}Fe nuclei along the direction of the incident x-ray beam [16]. It has been shown to provide a vibrational fingerprint of the FeMo-cofactor Fe_6S_9X core that is potentially sensitive to structure of the cluster [17,18].

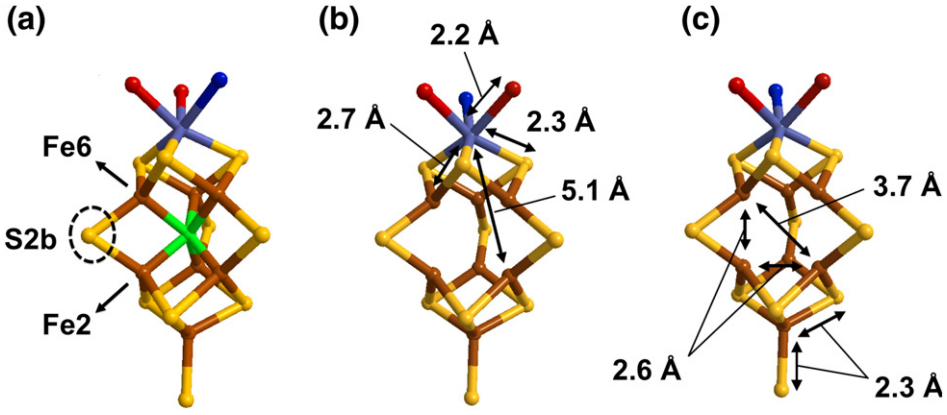

Scheme 2. The FeMo-cofactor showing (a) structural movements considered in the text, (b) distances important for Mo EXAFS and (c) distances important for Fe EXAFS. The interstitial atom "X" is omitted for clarity in (b) and (c). The atoms colors are given in Scheme 1.

Both XAS and NRVS have the enormous advantage of being applicable to frozen solutions enabling measurement of transient states.

In this paper, we present the first XAS and NRVS study of MoFe nitrogenase with a ligand bound to the FeMo-cofactor. Specifically we study the propargyl alcohol ($HC{\equiv}CH_2OH$, PA) bound state of the α-70^{Ala} variant of *Azotobacter vinelandii* (*Av*1) MoFe nitrogenase (*Av*1) [19–22]. This complex is formed on turnover with the PA substrate, and has been assigned to an allyl alcohol species coordinated to the FeMo-cofactor active site [19,20]. The complex has a characteristic $S = 1/2$ electron paramagnetic resonance (EPR) signal which allows it to be readily quantified. For this work, samples were generated by turning a mixture of α-70^{Ala} MoFe protein and Fe protein with ATP and sodium dithionite in the presence of PA (α-70^{Ala}:PA) or the absence of PA (α-70^{Ala}:turnover) and freezing rapidly. Control samples of the resting, dithionite reduced enzyme were also prepared (α-70^{Ala}:resting). For α-70^{Ala}:PA, EPR experiments were used to confirm the presence of high yields of the complex.

2. Experimental

2.1. Protein Purification and Sample Preparation

Azotobacter vinelandii α-70^{Ala} MoFe protein was prepared according to published procedures. For α-70^{Ala}:resting, the dithionite reduced enzyme was flash frozen in custom Lucite cuvettes. The turnover samples were made with a 1:0.75 ratio between the α-70^{Ala} MoFe protein (500 μM) and Fe protein in 75 mM MOPS, pH 7.0, 7.5 mM $MgCl_2$, 1 mg/mL creatine kinase, 5 mM ATP, 35 mM phosphocreatine, 30 mM sodium dithionite and when required, 15 mM propargyl alcohol. The MoFe protein was preincubated in the reaction mixture and turnover was initiated with the addition of the Fe protein. The reaction-initiated samples were quickly (~ 20 – 30 seconds) transferred into Lucite cuvettes and flash frozen. All manipulation was under strictly anaerobic conditions within crimp sealed vials that were repeatedly evacuated and back-filled with Ar and all solution transfers were with gas-tight syringes.

In order to assess the yield of α-70^{Ala}:PA we prepared EPR samples using the same solutions and quantitated the characteristic $S = 1/2$ signal. It was not possible to prepare the control EPR samples simultaneously with the EXAFS or NRVS samples because of the short reaction time before freezing. These EPR experiments reliably generated around 0.7 spins per Mo. As a separate control, we recovered EXAFS and NRVS samples after measurement, ground them under liquid nitrogen and packed the powder into EPR tubes. These experiments also yielded the intense α-70^{Ala}:PA EPR signals with intensities consistent with our EPR control measurements.

2.2. X-ray Absorption Spectroscopy

Mo and Fe K-edge x-ray absorption data were measured at Stanford Synchrotron Radiation Lightsource beamline 9–3, using a Si 220 double-crystal monochromator. Fluorescent x-rays were measured using a 30-element Ge fluorescence detector (Canberra Industries), fitted with Soller slits and a Zr (for Mo) or Mn (for Fe) filter to minimize the relative contribution of scattered radiation. An Oxford Instruments CF1208 liquid helium cooled sample cryostat was used to maintain the sample temperature at 9 K. The x-ray energy was calibrated using the first major inflection point of a standard Mo or Fe foil set as 20003.9 eV or 7111.3 eV respectively. This was measured at the same time as the sample spectrum using two ion chambers positioned downstream of the cryostat. In order to minimize the effect of x-ray photoreduction, the sample was moved after each scan so that the beam irradiated a different spot on the sample for each scan – typically a total of 3 – 4 spots were available for each sample and 5 – 11 scans were collected requiring reuse of each spot. For both Mo and Fe, the K-edge structure and position were monitored to ensure that no photochemistry occurred.

2.3. EXAFS data analysis

EXAFS data were analyzed using the EXAFSPAK suite of programs [23]. Curve fitting used the EXAFSPAK program OPT, with single-scattering phase and amplitude functions calculated using FEFF 7.0 [15].

Our approach was to fit the α-70^{Ala}:resting data first and use this fit to obtain a set of Debye-Waller factors which were then be fixed for the remaining data analysis. The number (N) of each interaction was fixed to the expected value from crystallography, with the exception of the short ~2.7 Å Fe-Fe interaction for which the number from P-cluster contribution was set to zero. This was because these interactions in the P-cluster have been reported to phase-cancel [24], and consistent with this we found increasing the Fe-Fe number (N) to 3 gave unreasonable Debye-Waller factors. Approximate distances (R) and Debye-Waller factors (mean square deviations – σ^2) were entered for each interaction. R, σ^2 and ΔE_0 were then allowed to float and the structure was optimized for a good fit. One problem for the Fe EXAFS analysis, is that the Fe-Mo interaction at ~2.7 Å tends to inversely correlate with the short Fe-Fe at ~2.6 Å, so the Fe-Mo σ^2 was fixed to the value derived from Mo EXAFS and not allowed to float. Once the Debye-Waller terms had been determined, these were fixed, and for each of the three states, including α-70^{Ala}:resting, N, R and ΔE_0 were allowed to float for the final fits presented here.

We note that some the expected values for the number (N) of the Fe EXAFS interaction are higher for α-70^{Ala}:resting compared to α-70^{Ala}:turnover and α-70^{Ala}:PA as the latter two samples contain a 1:0.75 ratio of the [4Fe-4S] cluster containing Fe protein whereas the α-70^{Ala}:resting samples do not. For example, the expected numbers for the Fe-Mo and long 3.7 Å Fe-Fe interactions are 0.2 and 0.8 respectively for α-70^{Ala}:resting and 0.182 and 0.727 when Fe protein is present.

2.4. NRVS Measurements

Samples for ^{57}Fe NRVS employed ^{57}Fe enriched MoFe protein. NRVS data were recorded using published procedures [16] at beamline BL09XU, SPring-8, Japan [25] and at beamline ID-3 at the Advanced Photon Source, Argonne, USA. Typical flux was ~3 x 10^9 in a 1.1 meV bandwidth (1 meV ≡ 8.0655 cm^{-1}). During NRVS measurements, the samples were maintained at ~20 K using a liquid He cryostat. Exact temperatures for individual spectra were calculated using the ratio of anti-Stokes to Stokes intensity according to: $S(-E) = S(E)\exp(-E/kT)$. Spectra were recorded between −20 meV and 80 meV in 0.25 meV steps. Nuclear fluorescence and Fe K fluorescence (from internal conversion) were recorded using an APD array [26]. Each scan typically took about 40 min, and all scans were added and normalized to the intensity of the incident beam.

2.5. Normal Mode Calculations

Normal mode calculations were conducted with a Urey-Bradley force field using a modification of the program 'Vibratz' [27]. Calculations used the previously published force constants and structural model for FeMo-cofactor [17] except that the symmetry was reduced to C_1 from C_{3v} to allow modifications at a single site. These calculations are detailed in the supplementary information. For comparison with experimental spectra, each calculated mode was multiplied by a Gaussian lineshape with 7 cm^{-1} full width at half maximum amplitude.

3. Results

Figs. 1 and 2 compare the XAS near-edge and EXAFS data from α-70^{Ala}:PA with α-70^{Ala}:turnover and α-70^{Ala}:resting. Fig. 1 presents the Mo K-edge spectra, with the upper panel comprising the Mo near-

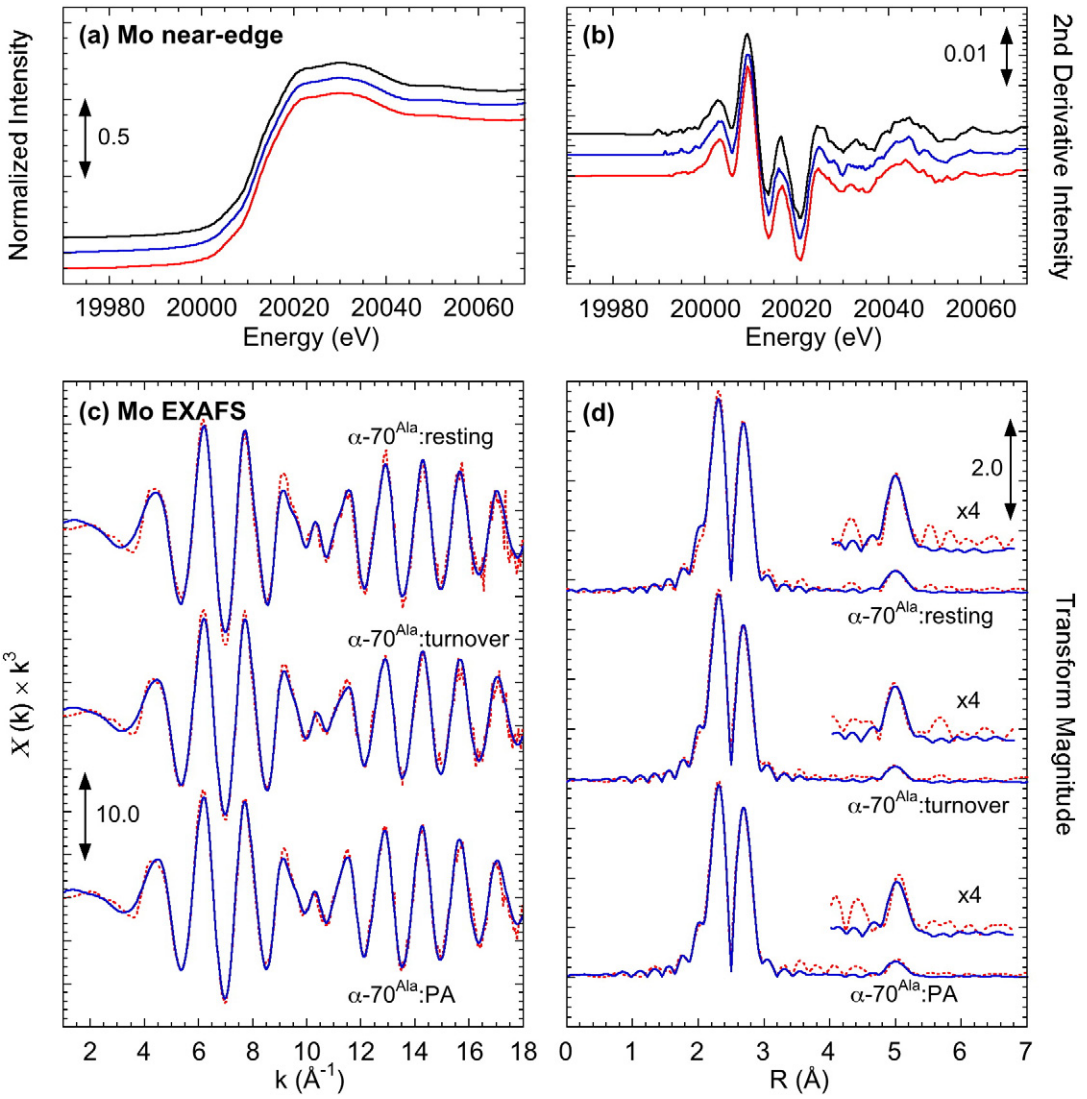

Fig. 1. Mo K-edge x-ray absorption spectroscopy of α-70^{Ala}:PA compared with α-70^{Ala}:turnover and α-70^{Ala}:resting. (a) near-edge spectra, (b) near-edge 2nd derivative spectra, (c) EXAFS spectra and (d) EXAFS Fourier transform spectra phase corrected for Mo-S. In each panel: upper spectrum - α-70^{Ala}:resting; center spectrum - α-70^{Ala}:turnover; lower spectrum - α-70^{Ala}:PA. In (c) and (d) broken line - data; solid line – fit.

edge spectra and second derivatives while the lower panel comprises the Mo EXAFS spectra and Fourier transforms superimposed by curve fitting results. Fig. 2 similarly compares the Fe K-edge near-edge spectra and the Fe EXAFS with analysis. Fig. 3 compares the NRVS spectra of α-70^{Ala}:PA with the published wild-type spectrum and some simulated spectra. The EXAFS fitting parameters are presented in Table 1, while complete EXAFS fitting parameters together with details for the NRVS simulations are presented in the supplementary information.

We note that the EPR control experiments indicate that the α-70^{Ala}:PA EXAFS and NRVS samples contained at least 0.7 of the bound PA form per FeMo-cofactor. It is important to realize this represents a minimum yield of bound complex. This is because the EPR spectra obtained from α-70^{Ala}:PA typically did not contain intense signals corresponding to unbound active site, which allows the possibility that the remaining 0.3 FeMo-cofactor could also comprise bound PA but in an EPR silent state.

We first consider the Mo near-edge XAS data and the Mo EXAFS and whether there is any suggestion of PA binding at Mo (Fig. 1 and Table 1). The near-edge spectra from α-70^{Ala}:resting, α-70^{Ala}:turnover and α-70^{Ala}:PA (Fig. 1a,b) are virtually superimposable. As near-edge structure predominately arises from transitions to states that are sensitive to the Mo oxidation state, ligand field and geometry, this suggests the Mo oxidation state and ligand field is similar in all three cases. Similarly, analyses of Mo EXAFS of these two states (Fig. 1c,d and Table 1) do not show substantial differences in the shells of the coordinating ligands. The EXAFS data are of high quality, showing very good signal to noise, enabling measurement up to k = 18 Å^{-1}. Curve fitting analyses reveal the expected Mo-S and Mo-Fe interactions at 2.37 Å and 2.69 Å respectively, as well as the long Mo-Fe interaction at 5.10 Å (Scheme 2b). The shorter Mo-O and Mo-N ligands, fitted as 3 Mo-O interactions, are also apparent, although these are weaker compared to the Mo-S and shorter Mo-Fe interaction comprising just over 13% of the total EXAFS. Nevertheless, any binding of PA should introduce Mo-C interactions that would modulate the Mo-O fit. As Table 1 indicates, there is very little change in this interaction between the resting enzyme, the enzyme under turnover and the enzyme with bound PA. Hence, taken together, the Mo EXAFS and near-edge data do not suggest binding of PA at the Mo site.

There are some minor changes in the Mo EXAFS of each state that involve the Mo-Fe interactions. For the short 2.7 Å Mo-Fe interaction there is a small (10%) reduction in intensity of the α-70^{Ala}:turnover compared to the other two states. Of particular interest, however, is

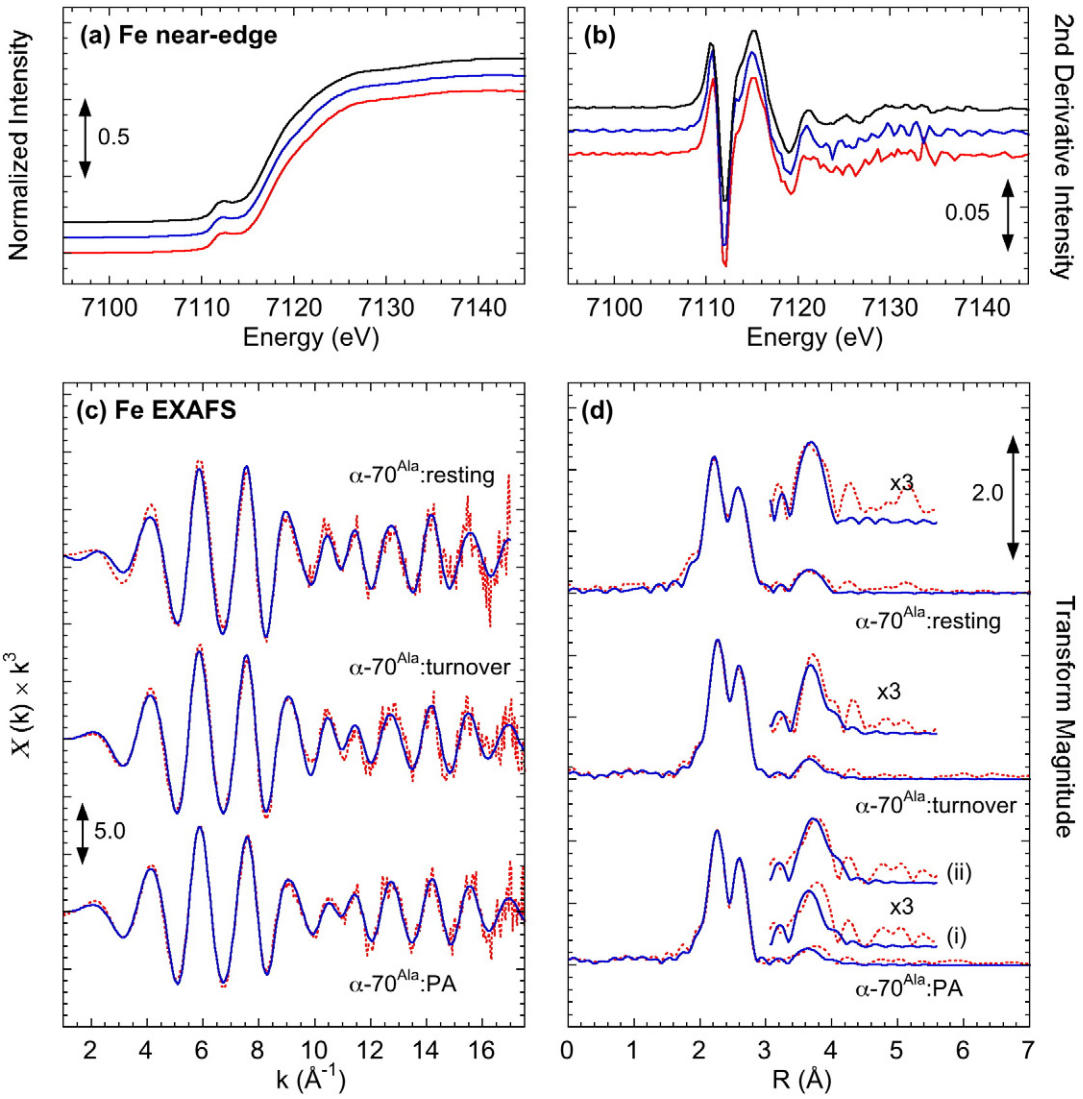

Fig. 2. Fe K-edge x-ray absorption spectroscopy of α-70^{Ala}:PA compared with α-70^{Ala}:turnover and α-70^{Ala}:resting. (a) near-edge spectra, (b) near-edge 2nd derivative spectra, (c) EXAFS spectra and (d) EXAFS Fourier transform spectra phase corrected for Fe-S. In each panel: upper spectrum - α-70^{Ala}:resting; center spectrum - α-70^{Ala}:turnover; lower spectrum - α-70^{Ala}:PA. In (c) and (d) broken line - data; solid line - fit. (i) and (ii) in (d) are different fits for α-70^{Ala}:PA as described in the text.

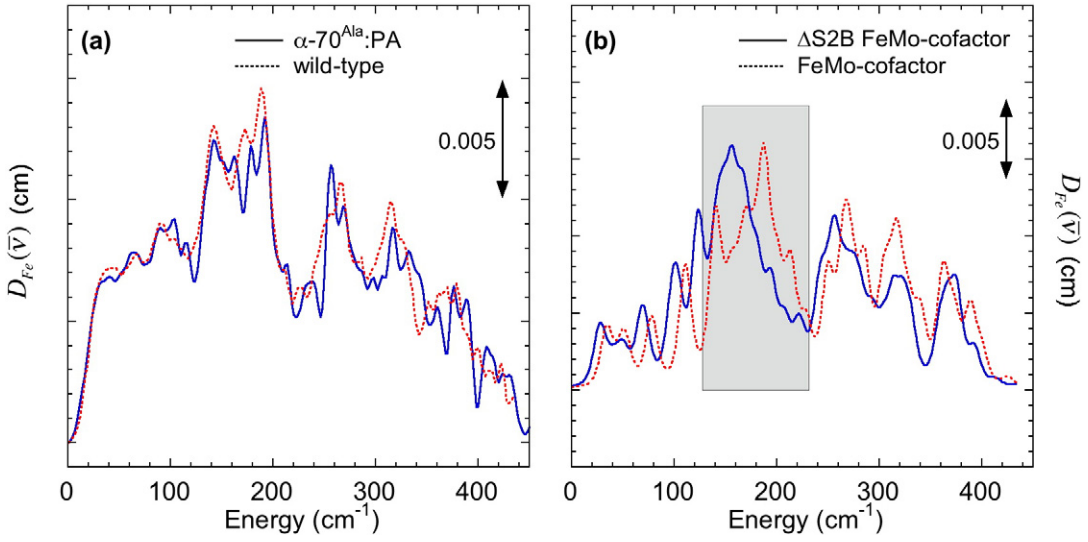

Fig. 3. NRVS results. (a) NRVS spectrum of α-70^{Ala}:PA (solid line) compared with resting wild-type *Av*I (broken line). (b) Calculated NRVS spectra showing the possible effect of opening the Fe_6S_9X core simulated by deleting S2b (solid line) compared with that calculated for unmodified FeMo-cofactor (broken line). The calculations do not include the P-cluster. The shaded region is discussed in the text.

Table 1
EXAFS fitting parameters[a].

	α-70^{Ala}: resting		α-70^{Ala}: turnover		α-70^{Ala}:PA		
	N[b]	R (Å)[b]	N	R (Å)	N	R (Å)	σ^2 (Å^2)[c]
Mo-S	2.95	2.372	2.97	2.375	2.91	2.373	*0.00212*
Mo-Fe	3.00	2.694	2.73	2.690	2.97	2.697	*0.00303*
Mo-Fe	3.03	5.101	2.47	5.096	2.51	5.108	*0.00560*
Mo-O	3.13	2.190	2.85	2.191	2.88	2.195	*0.00307*
Fe-S	3.66	2.295	3.76	2.300	3.57	2.287	*0.00563*
Fe-Fe	1.65	2.615	1.57	2.617	1.44	2.618	*0.00371*
Fe-Fe	0.38	2.846	0.51	2.840	0.35	2.827	*0.00371*
Fe-Mo	*0.20*	2.687	*0.18*	2.664	*0.18*	2.686	*0.00303*
Fe-Fe (long) (i)	0.82	3.705	0.75	3.705	0.63	3.700	*0.00300*
Fe-Fe (long) (ii)					0.59	3.701	*0.00300*
Fe-Fe (long) (ii)					0.22	3.985	*0.00300*

[a] Complete fitting parameters are in the supplementary information. Fixed values are in italics.
[b] N = number of backscattering atoms. R = distance.
[c] σ^2 = Debye-Waller factor or mean-square deviation in distance. These were constrained to the same values for all samples.

the long Mo-Fe interaction at 5.10 Å. This arises from the 3 Fe atoms on the distal side of the Fe_6S_9X core of the FeMo-cofactor from the Mo terminus (Scheme 2b) and it should be sensitive to conformational deformations of the Fe_6S_9X core. We note that fitted distance of this interaction is essentially the same in all three states. However, the intensity of this feature in both the α-70^{Ala}:turnover and α-70^{Ala}:PA states is reduced by ~16% compared to α-70^{Ala}:resting. Interestingly, comparing α-70^{Ala}:turnover and α-70^{Ala}:PA shows there is no additional difference in this interaction caused by the bound PA product.

The reduction in intensity of the 5.1 Å Mo-Fe interaction on turnover is most easily rationalized in terms of a conformational deformation of the cluster that results in small, unresolved changes in the long Mo-Fe distances. Similarly, the lack of any further difference in this interaction between α-70^{Ala}:turnover and α-70^{Ala}:PA suggests that any conformational change caused by the bound PA product does not significantly alter the long Mo-Fe interaction. Clearly, any large atom movement that produces a substantial change in one of the Mo-Fe distances would cause the Fourier transform of this interaction to be split into two peaks. However, if the change in the Mo-Fe distance is less than the EXAFS resolution of π/2Δk, here 0.09 Å, then the two distances cannot be resolved by curve fitting and instead the heterogeneity in distance adds to the static component of the Debye-Waller factor, which in turn results in a single average distance with an increased Debye-Waller factor. However, our analytical approach for this work, detailed in the experimental section, uses the same, fixed, Debye-Waller factors to fit each of the α-70^{Ala}:resting, α-70^{Ala}:turnover and α-70^{Ala}:PA states and only distance, number and ΔE_0 are allowed to float. Since increasing the Debye-Waller factor reduces the intensity of the observed EXAFS, it tends to inversely correlate with the number of interactions present, which in turn means that any unresolved increase in heterogeneity of the 5.1 Å Mo-Fe interaction will result in a single observed interaction but with a smaller fitted number. This is observed in the curve fits presented here from the α-70^{Ala}:resting and the two turnover samples. We note that the most likely explanation for this difference is that under turnover a mixture of FeMo-cofactor oxidation states is present and that these exhibit slightly different geometries. This is consistent with known biochemistry of the nitrogenase enzyme complex [1], the almost negligible changes in the 5.10 Å average fitted distances (< 0.015 Å) as well as the observation that the Fe EXAFS does not show a corresponding increase in heterogeneity in the 3.7 Å Fe-Fe interaction (see below). We also note that the near identity of the 5.1 Å Mo-Fe interaction in the α-70^{Ala}:turnover and α-70^{Ala}:PA states strongly indicates that there is no further significant geometric change at these distal Fe sites in the bound form of PA.

We now consider the Fe near-edge XAS data and the Fe EXAFS (Fig. 2 and Table 1). The Fe near-edge spectra of all three states are visually similar (Fig. 2a), with only subtle differences around the pre-edge feature at 7112 eV apparent in the second derivative spectra (Fig. 2b). This lack of significant change between these spectra was not unexpected as unlike Mo, with its single unique site, there are 15 different Fe sites in each MoFe enzyme. The change in overall Fe oxidation state in MoFe nitrogenase under the turnover conditions here is expected to average approximately only one electron reduction amongst the 15 Fe, making any shift in the K-edge correspondingly small. Similarly, any changes resulting from PA product coordination to Fe will probably be similarly diluted, as the PA product is unlikely to coordinate more than two Fe sites. Finally, any differences between α-70^{Ala}:resting and the two turnover states and can be ascribed to the presence of the [4Fe-4S] cluster containing Fe protein in the latter two samples.

Fortunately the Fe EXAFS data are very informative (Fig. 2c-d). Again, the spectra are of high quality, with good signal to noise throughout the k < 17 Å^{-1} range of the measured data. Curve fitting analysis reveals that the Fe EXAFS is dominated by the expected short range Fe-S and Fe-Fe interactions (Scheme 2c). These are fitted for the α-70^{Ala}:resting spectrum at 2.30 Å and 2.62 Å respectively. We note that fitting these components is complicated by the presence of the P-cluster and Fe protein in the sample as both of these can contribute similar Fe-S and Fe-Fe interactions. For the fits in Fig. 2 a Fe-Fe contribution from the P-cluster has not been included as it has been reported that this tends to be small due to phase-cancellation effects [24], resulting in a low number of fitted Fe-Fe interactions per Fe (Table 1) as these are averaged over all the Fe in the sample. Interestingly, the fits are significantly improved by including a small Fe-Fe contribution at ~2.84 Å and we note that the origin of this component is unclear as it could arise from either the P-cluster or the FeMo-co active site. The Fe-Mo interaction at 2.69 Å tends to inversely correlate with the short Fe-Fe interaction, so its intensity is fixed at the expected values of 0.2 for α-70^{Ala}:resting and 0.182 for the turnover samples. The final component of the each of the Fe EXAFS spectra is the long Fe-Fe interaction which occurs at 3.71 Å in α-70^{Ala}:resting. This interaction is characteristic of the Fe_6S_9X core of the FeMo-cofactor [18], and it arises from the diagonal across the square faces of the trigonal prism (Scheme 2c).

A comparison of the Fe EXAFS from each of the three sample states (α-70^{Ala}:resting, α-70^{Ala}:turnover, α-70^{Ala}:PA) shows clear and reproducible differences in the long 3.7 Å Fe-Fe interaction for the PA bound form. For the short Fe-S and Fe-Fe interactions there are only limited differences between the three states, with distances in particular being very comparable. Similarly, the reduction in number (N) of the long 3.7 Å Fe-Fe interaction between α-70^{Ala}:resting and α-70^{Ala}:turnover is from 0.82 to 0.75 per Fe, almost exactly the 0.8 to 0.73 expected from the diluting effect of the added Fe protein. However, the addition of PA causes the intensity of this feature to further reduce together with a significant change in the shape of its Fourier transform. This is reflected in the curve-fitting analysis. For both α-70^{Ala}:resting and α-70^{Ala}:turnover, this interaction fits well to single bands at 3.71 Å, while for the α-70^{Ala}:PA spectrum, constraining the analysis to a similar interaction produces a relatively poor fit with reduced intensity, as illustrated as fit (i) in Table 1 and Fig. 2d. It is important to note that the Debye-Waller factors for the α-70^{Ala}:PA fit were fixed to the fitted values from the α-70^{Ala}:resting analysis, so any structural changes are reflected in the number and distance of each type of interaction only. Finally, we investigated the impact of introducing an additional long-range Fe-Fe component into the fit for the PA spectrum. This part of the analysis requires two important caveats. First, care must be taken when fitting these relatively weak long-range interactions as this region also includes normally unresolved Fe-S interactions. Second, introducing additional components nearly always improves the fit quality and when introducing weak features care must be made not to overinterpret the results.

Nevertheless, we found that for the PA spectrum, this fit is significantly improved by including an additional smaller Fe-Fe interaction at 3.99 Å; shown as fit (ii) in Table 1 and Fig. 2d.

The most straightforward interpretation of this observation is that PA is binding to a Fe site on FeMo-cofactor, with a concomitant distortion of the Fe_6S_9X core, which in turn modifies some of the long Fe-Fe interactions. The Mo EXAFS data are relevant here as it is clear from Scheme 2b that the short 2.7 Å Mo-Fe and long 5.1 Å Mo-Fe should also be sensitive to conformational distortions of the Fe_6S_9X core. It is interesting to note that, on comparing α-70^{Ala}:turnover and α-70^{Ala}:PA, the short Mo-Fe shows a slight (9%) increase in number on binding PA while the long Mo-Fe interaction is essentially unchanged. We also note that the curve fitting analysis does not provide any direct indication of the presence of any Fe-C interactions from PA bound to a Fe site. This is not unexpected. Fe-C interactions are inherently weak and the presence of additional Fe from the P-cluster and Fe protein Fe_4S_4 cluster will further dilute any Fe-C interaction so that the expected number value (N) for side-on bound PA complex is only 0.13. Hence, in this case they most likely are overwhelmed by the more intense 2.30 Å Fe-S and 2.61 Å Fe-Fe interactions.

The simplest chemically consistent structural change that accounts for these data is that PA binds to one of the Fe atoms (Fe5, Fe6, Fe7) adjacent to the Mo terminus, with a concomitant movement of the Fe away from the central atom X and along the Fe-X bond. This movement is expected to modify the long 3.7 Å Fe-Fe interaction, but not the long 5.1 Å Mo-Fe distances. We exclude the analogous binding at a Fe adjacent to the Fe terminus (Fe2, Fe3, Fe4), as, although this would be expected to cause the same modification of the long Fe-Fe, it should also similarly affect the long Mo-Fe, and this is not observed. Any more substantial modification of the cluster, such as breaking Fe-S bonds within the Fe_6S_9X core would also most likely significantly modify the long Mo-Fe interaction. If the 3.99 Å Fe-Fe interaction observed in fit (ii) in fact represents the moved Fe atom, this would represent a lengthening of Fe-X by about 0.35 Å. In this case, the apparent increase in the total number for the long Fe-Fe can be rationalized in terms of a reduction in the static Debye-Waller factor for both components. The expected sensitivity of EXAFS measurements to conformational changes in the FeMo-cofactor is detailed in the supplementary information.

Further insight into the nature of the conformational change on PA binding is provided by NRVS measurements. We note that these spectra again contain contributions from both the FeMo-cofactor and the P-cluster. Fig. 3a compares the ^{57}Fe NRVS spectrum of α-70^{Ala}:PA with that previously published for resting wild-type MoFe nitrogenase [17]. While there are intensity differences in some of the bands, both spectra are very similar, with the most noticeable differences being a small general reduction in intensity between 140 – 200 cm^{-1} as well as some details throughout the spectrum. We note, as with Fe EXAFS, we are unlikely to directly observe any Fe-C coordination from a bound ligand with the current data. This is for two reasons. First, these modes will likely affect only one Fe, so the other Fe in the sample will dilute their intensity. Second, Fe-C modes are in general inherently weaker than the Fe-S modes that dominate the NRVS spectrum of MoFe nitrogenase. NRVS intensity in a given vibrational mode is directly related to the magnitude of the overall Fe motion in that mode, hence heavier ligands, like S, will normally give more intense NRVS than lighter coordinating atoms, such as C.

In order to better understand the significance of this result we adapted the existing empirical normal mode analysis for the FeMo-cofactor [17] to a C_1 coordinate frame and explored the impact of structural changes of the cluster on the NRVS spectrum. The key result is presented in Fig. 3b. Moving individual Fe atoms by distances less than 0.5 Å caused relatively minor changes in the spectrum (not shown). The most significant change was caused by opening the Fe_6S_9X core, simulated by deleting the bridging S2b atom (Scheme 2a), which substantially reduces the intensity of the bands between 180 – 220 cm^{-1} while increasing intensity between 140 – 170 cm^{-1} (shaded area on Fig. 2b). This is not unexpected, as the bands between 180 – 220 cm^{-1} are assigned to breathing vibrations of the Fe_6S_9X core [17]; a motion which depends on the presence of the interstitial atom X and the integrity of the core. Opening the core apparently eliminates these modes, and the cluster behaves more like a pair of FeS cubanes, which have breathing modes at around 145 cm^{-1} [28]. Hence we conclude that there has not been a substantial change in the structure of the FeMo-cofactor involving breaking the μ^2 Fe-S-Fe bonds of the Fe_6S_9X core as has been suggested possible from DFT calculations [9–12] and that the structure of the Fe_6S_9X core remains essentially intact.

4. Discussion and Conclusions

This XAS and NRVS study comprises the first experimental evidence of the conformational changes of the FeMo-cofactor active site on binding a substrate or product. The primary conclusion is that the bound form of PA formed under turnover induces only a small change in the cofactor. The EXAFS data are consistent with the movement of a single core Fe along the Fe-X bond and away from the interstitial X. It allows us to localize this change to a Fe adjacent to the Mo terminus. Both the EXAFS and NRVS data argue against any substantial change in the cluster structure, such as opening the Fe_6S_9X core through breaking Fe-S bonds. This study also provides evidence binding is not at the Mo site. Finally, while any estimate must be treated with care as it depends on fitting weak components in a complex spectrum, it allows us to estimate of the magnitude of the Fe atom movement to be about 0.35 Å.

We thus conclude that the PA binding site is Fe6 or Fe7 as illustrated in Scheme 3. The reasonable assumption that the Fe movement is a consequence of a bound PA ligand limits binding to one of Fe5, Fe6 or Fe7. We can exclude the Fe5 site as recent experiments have emphasized the importance of the Fe2-3-6-7 face to substrate binding [20–22,29–31]. This conclusion is consistent with an electron nuclear double resonance (ENDOR) and DFT analysis, which has assigned the complex to a side-on bound η^2-alkene or metallocyclopropane allyl alcohol bound at Fe6 and stabilized by hydrogen bonding of the alcohol group with the α-195^{His} residue [19,20].

A secondary conclusion from this study concerns our methodology. This work demonstrates that EXAFS and NRVS are highly complementary techniques for studying Fe sites and in particular Fe containing metal clusters in biological systems. For MoFe nitrogenase, EXAFS is a sensitive tool for monitoring conformational changes in the FeMo-cofactor and providing structural details of those changes, while NRVS provides

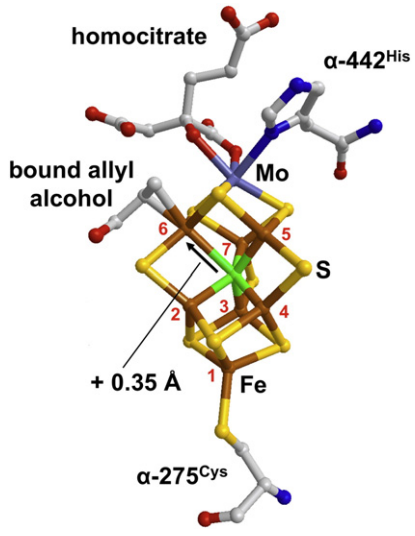

Scheme 3. The FeMo-cofactor showing the proposed structure of the PA bound form consistent with the EXAFS and NRVS analysis. The atoms colors are given in Scheme 1.

the necessary check of overall cluster integrity. Although, in this case, the large number of additional Fe atoms in the samples prevented the bound PA from being directly observed, both techniques have the capability of detecting and confirming the presence of bound ligands; EXAFS through direct measurement of the metal-ligand distance and NRVS through measurement of the associated stretching and bending vibrational modes. Finally, both techniques require very similar sample concentrations and preparation, although it is important to remember that NRVS requires ^{57}Fe enrichment. Indeed, with careful experimental design, the same sample could be used for both NRVS and XAS experiments.

Finally, the fact that we do not observe a major change in the FeMo-cofactor in the PA bound form also deserves some comment. We note that DFT models that predict opening the Fe_6S_9X core calculate reduced forms of the cofactor. By corollary, our observation that this change is absent implies that the cofactor is not in a significantly reduced state. Since α-70^{Ala}:PA has an $S = 1/2$ EPR signal, the cluster must be either in its resting state or reduced by a multiple of 2 electrons. We therefore suggest that the PA bound complex studied here is a product bound state with the cofactor at the same overall oxidation state as the resting enzyme. This conclusion is consistent with the relatively long lifetime of this state. We also note that other stable substrate-bound intermediates either may well have the FeMo-cofactor in a more reduced state, such as the α-70$^{Ala}\alpha$-195^{Gln} hydrazine complex [32], or may involve multiply bound ligands, such as the wild-type Hi-CO complex [31,33]. These may well induce a more significant change in cluster conformation. A combined XAS and NRVS study of these species will undoubtedly be of great interest.

Note added in proof

During publication of this article two papers were published suggested that the interstitial atom X is in fact carbon.

T. Spatzal, M. Aksoyoglu, L. Zhang, S.L.A. Andrade, E. Schleicher, S. Weber, D.C. Rees, O. Einsle, Science 334 (2012) 940.

K.M. Lancaster, M. Roemelt, P. Ettenhuber, Y. Hu, M.W. Ribbe, F. Neese, U. Bergmann, S. DeBeer, Science 334 (2012) 974-977.

Acknowledgments

This work was funded by NIH GM-65440 (SPC), GM-59087 (LCS and DRD) and NSF CHE-0745353 (SPC). ABEX is supported by the U.S. Department of Energy, Office of Biological and Environmental Research (DOE OBER). Portions of this research were carried out at the Stanford Synchrotron Radiation Lightsource (SSRL), a national user facility operated by Stanford University on behalf of the DOE Office of Basic Energy Sciences (OBES). The SSRL Structural Molecular Biology Program is supported by the DOE OBER, and the NIH, National Center for Research Resources, Biomedical Technology Program. Portions of this work were also carried out at SPring-8 with the approval of the Japan Synchrotron Radiation Research Institute (JASRI) under Proposal # 4032LD3-NP. Use of the Advanced Photon Source was supported by the DOE OBES under Contract No. DE-AC02-06CH11357.

Appendix A. Supplementary data

Full EXAFS fitting parameters; details of the sensitivity of EXAFS distances to Fe-X movements in FeMo-cofactor; NRVS simulation parameters. Supplementary materials related to this article can be found online at doi:10.1016/j.jinorgbio.2012.02.004.

References

[1] B.K. Burgess, D.J. Lowe, Chem. Rev. 96 (1996) 2983–3011.
[2] J.W. Peters, R.K. Szilagyi, Curr. Opin. Chem. Biol. 10 (2006) 101–108.
[3] O. Einsle, F.A. Tezcan, S.L.A. Andrade, B. Schmid, M. Yoshida, J.B. Howard, D.C. Rees, Science 297 (2002) 1696–1700.
[4] D.C. Rees, F.A. Tezcan, C.A. Haynes, M.Y. Walton, S. Andrade, O. Einsle, J.B. Howard, Philos. Trans. R. Soc. A 363 (2005) 971–984.
[5] R.Y. Igarashi, L.C. Seefeldt, Crit. Rev. Biochem. Mol. Biol. 38 (2003) 351–384.
[6] L.C. Seefeldt, B.M. Hoffman, D.R. Dean, Annu. Rev. Biochem. 78 (2009) 701–722.
[7] D. Lukoyanov, Z.Y. Yang, D.R. Dean, L.C. Seefeldt, B.M. Hoffman, J. Am. Chem. Soc. 132 (2010) 2526–2527.
[8] L.C. Seefeldt, I.G. Dance, D.R. Dean, Biochemistry 43 (2004) 1401–1409.
[9] U. Huniar, R. Ahlrichs, D. Coucouvanis, J. Am. Chem. Soc. 126 (2004) 2588–2601.
[10] I. Dance, J. Am. Chem. Soc. 126 (2004) 11852–11863.
[11] J. Kaestner, P.E. Bloechl, Inorg. Chem. 44 (2005) 4568–4575.
[12] J. Kaestner, P.E. Bloechl, J. Am. Chem. Soc. 129 (2007) 2998–3006.
[13] R. Henderson, Chem. Rev. 105 (2005) 2365–2437.
[14] G.N. George, I.J. Pickering, in: V. Tsakanov, H. Wiedemann (Eds.), Brilliant Light in Life and Materials Sciences, Springer, Dordrecht, NL, 2007, pp. 97–119.
[15] J.J. Rehr, R.C. Albers, Rev. Mod. Phys. 72 (2000) 621–654, http://leonardo.phys.washington.edu/feff/.
[16] W. Sturhahn, J. Phys. Condens. Matter 16 (2004) S497–S530.
[17] Y. Xiao, K. Fisher, M.C. Smith, W. Newton, D.A. Case, S.J. George, H. Wang, W. Sturhahn, E.E. Alp, J. Zhao, Y. Yoda, S.P. Cramer, J. Am. Chem. Soc. 128 (2006) 7608–7612.
[18] S.J. George, R.Y. Igarashi, Y. Xiao, J.A. Hernandez, M. Demuez, D. Zhao, Y. Yoda, P.W. Ludden, L.M. Rubio, S.P. Cramer, J. Am. Chem. Soc. 130 (2008) 5673–5680.
[19] H. Lee, R.Y. Igarashi, M. Laryukhin, P. Doan, P.C. Dos Santos, D.R. Dean, L.C. Seefeldt, B.M. Hoffmann, J. Am. Chem. Soc. 126 (2004) 9563–9569.
[20] R. Igarashi, P. Dos Santos, W. Niehaus, I. Dance, D.R. Dean, L.C. Seefeldt, J. Biol. Chem. 279 (2004) 34770–34775.
[21] P. Benton, M. Laryukhin, S. Mayer, B.M. Hoffmann, D.R. Dean, L.C. Seefeldt, Biochemistry 42 (2003) 9102–9109.
[22] P.C. Dos Santos, S. Mayer, B.M. Barney, L.C. Seefeldt, D.R. Dean, J. Inorg. Biochem. 101 (2007) 1642–1648.
[23] G.N. George, S.J. George, I.J. Pickering, Stanford Synchrotron Radiation Laboratory, 1998; http://ssrl.slac.stanford.edu/exafspak.html.
[24] M.C. Corbett, Y. Hu, F. Naderi, M.W. Ribbe, B. Hedman, K.O. Hodgson, J. Biol. Chem. 279 (2004) 28276–28282.
[25] Y. Yoda, M. Yabashi, K. Izumi, X.W. Zhang, S. Kishimoto, S. Kitao, M. Seto, T. Mitsui, T. Harami, Y. Imai, S. Kikuta, Nucl. Instrum. Meth. A 467 (2001) 715–718.
[26] S. Kishimoto, Y. Yoda, M. Seto, S. Kitao, Y. Kobayashi, R. Haruki, T. Harami, Nucl. Instrum. Meth. A 513 (2004) 193–196.
[27] E. Dowty, Phys. Chem. Miner. 14 (1987) 67–79, http://www.shapesoftware.com.
[28] Y. Xiao, M. Koutmos, D.A. Case, D. Coucouvanis, H. Wang, S.P. Cramer, Dalton Trans. (2006) 2192–2201.
[29] B.M. Barney, R.Y. Igarashi, P.C. Dos Santos, D.R. Dean, L.C. Seefeldt, J. Biol. Chem. 279 (2004) 53621–53624.
[30] R. Sarma, B.M. Barney, S. Keable, D.R. Dean, L.C. Seefeldt, J.W. Peters, J. Inorg. Biochem. 104 (2010) 385–389.
[31] Z.-Y. Yang, L.C. Seefeldt, D.R. Dean, S.P. Cramer, S.J. George, Angew. Chem. Int. Ed. 50 (2011) 272–275.
[32] B.M. Barney, M. Laryukhin, R.Y. Igarashi, H.-I. Lee, P.C.D. Santos, T.-C. Yang, B.M. Hoffman, D.R. Dean, L.C. Seefeldt, Biochemistry 44 (2005) 8030–8037.
[33] H.-I. Lee, L.M. Cameron, B.J. Hales, B.M. Hoffman, J. Am. Chem. Soc. 119 (1997) 10121–10126.